



Effects of periodically kicked Dirac mass term in the Chern insulators

Fei Yang ^{1,2} Zheng Wei ¹ Tian-Meng Li,¹ and Su-Peng Kou^{1,*}

¹Center for Advanced Quantum Studies, Department of Physics, Beijing Normal University, Beijing 100875, China

²State Key Laboratory of Low Dimensional Quantum Physics, Department of Physics, Tsinghua University, Beijing 100084, China



(Received 13 November 2023; accepted 23 April 2024; published 7 May 2024)

Floquet engineering offers a unique approach to generate nonequilibrium topological phases in which the unbounded nature of a quasienergy band allows two kinds of topological edge modes, one of them traversing the 0 gap and another one traversing the π gap. Characterizing of these two modes is the main topic of Floquet topological insulators, where they are usually characterized by different topological invariants. However, in this paper, for a specific protocol of Floquet engineering where the Dirac mass term of the Chern insulator is periodically kicked, its topological phases are characterized with the Floquet Chern number C_F . Specifically, in our illustrative example, the periodically kicked Qi-Wu-Zhang model, there are six different topological phases in total, denoted as $C_F = \{-1_0, -2, -1_\pi, 1_\pi, 2, 1_0\}$. Topological phases with larger topological number are observed, i.e., $C_F = \pm 2$, where the chiral edge modes traversing the 0 gap and those traversing π gap have the opposite chirality. The mechanism of its topology is revealed by studying the corresponding low-energy effective Dirac Hamiltonian, and the phase boundaries between different topological phases are explicitly found. Additionally, we investigate the orders of phase transitions between different topological phases by studying the von Neumann entropy of the Floquet steady state (FSS), where the FSS corresponds to a stationary state of the Floquet system that is coupled to a Markovian environment. The hallmark of a periodically kicked Dirac mass term is uncovered in this paper, which may inspire further explorations of the physical effects of periodically kicked Dirac mass terms in other systems.

DOI: [10.1103/PhysRevB.109.195123](https://doi.org/10.1103/PhysRevB.109.195123)

I. INTRODUCTION

Topological phases are a class of states that have a robust conducting edge or surface modes, such as topological insulators (TIs) and topological superconductors [1]. Despite these static systems, engineering topological phases of matter with periodic driving is also an important field, called the Floquet system, in which the topological properties could be either analogous or beyond its static counterpart [2]. Many interesting phenomena are allowed in the periodically driven systems, such as Floquet-Anderson insulators [3,4], Floquet fractional Chern insulators [5], anomalous chiral edge states in periodically driven systems [6], and extraordinary topological phases in non-Hermitian Floquet systems [7–12].

The topological properties of periodically driven systems are reflected by their Floquet operators [13,14], which corresponds to the generators of a time-evolution operator over one period of driving, and its eigenvalue spectrum gives the corresponding Floquet-Bloch band [15,16]. Interestingly, the Floquet-Bloch band is unbounded, where one would expect to have two inequivalent quasienergy gaps, the zero-quasienergy gap (0 gap) and the π -quasienergy gap (π gap) [13], and they are usually characterized with different topological invariants [6,17]. Interestingly, the topological invariant of the Floquet-Bloch band may become anomalous in some Floquet Chern insulators, and edge modes exist even though the topological

number of the Floquet-Bloch band is zero. In this paper we find that the anomalous occurs only if the edge modes that traverse the 0 gap (0 modes) and those traversing the π gap (π modes) possess the same chirality, while the anomalous is absent if they have opposite chirality.

In this paper the topological phases of periodically kicked Chern insulators are studied in detail, where its Dirac mass term is periodically kicked. We find that the anomalous is absent, which is because the chirality of 0 modes is opposite to the chirality of π modes. So the Floquet Chern number C_F is sufficient to characterize the topology of those systems. In the illustrative example, the periodically kicked Qi-Wu-Zhang (PK-QWZ) model, there are six different topological phases in total, which corresponds to $C_F = \{-1_0, -2, -1_\pi, 1_\pi, 2, 1_0\}$. In the low-energy limit, the Floquet operator of the PK-QWZ model reduces to a Dirac Hamiltonian, which shares a similar algebraic structure with its static counterpart. This insight allows us to establish the phase diagram by identifying the number of skyrmions in the Floquet-Bloch band, and the transition lines between different topological phases are explicitly found.

Beyond its topological structure, we also investigate the orders of phase transition (OPT) between different topological phases. The main problem is to find its ground state, which is not a well-defined problem because the Hamiltonian is time dependent. In this paper, such difficulties are resolved by considering the steady state of the open quantum system, which is analogous to the ground state of the static system. We consider the situation where the PK-QWZ model is coupled to

*spkou@bnu.edu.cn

a Markovian environment in a specific way; then the system will relax into a stationary state, called the Floquet steady state (FSS). Finally, we can determine the OPT between different topological phases in the PK-QWZ model by investigating the von Neumann entropy of the FSS.

This paper is organized as follows. We briefly review the concepts of the Floquet system in Sec. II. Then, in Sec. III we introduce the PK-QWZ model, in which its Dirac mass term is periodically kicked, and the corresponding topology is characterized by the Chern number of the Floquet-Bloch band, C_F . In Sec. IV we study the topological phase diagram of the PK-QWZ model, in which the number of skyrmions within the Floquet-Bloch band is identified, and the phase boundaries are explicitly found. In Sec. V we consider a situation where the PK-QWZ model is coupled to the Markovian environment in a specific way in which the OPT between different topological phases are found by investigating the von Neumann entropy of FSS. We conclude our work in Sec. VI, and some future directions are discussed as well. The lengthy derivations are provided in the Appendixes. Appendix A corresponds to the expression of the Floquet operator for the PK-QWZ model, and Appendix B corresponds to the matrix equation of FSS for the free fermionic systems that are coupled to a Markovian environment.

II. THE PERIODICALLY DRIVEN QUANTUM SYSTEMS

The temporal evolution of a system that has a time-dependent Hamiltonian is quite intricate. Nevertheless, this complexity is significantly reduced when the Hamiltonian is periodic in time, denoted as $H(t + T) = H(t)$. That long-time behavior of the system can be characterized by a stroboscopic time-evolution operator

$$U(T) = \hat{\mathcal{T}} \exp \left(-i \int_t^{t+T} H(t') dt' \right), \quad (1)$$

in which the Floquet state $|\psi_{\epsilon_F}\rangle$ of the system only picks up a phase factor $e^{-i\epsilon_F T}$ over one complete period of driving [18], in other words,

$$U(T)|\psi_{\epsilon_F}\rangle = e^{-i\epsilon_F T} |\psi_{\epsilon_F}\rangle. \quad (2)$$

From a stroboscopic point of view, $|\psi_{\epsilon_F}\rangle$ plays the role of stationary states of $U(T)$ and with eigenvalues $e^{-i\epsilon_F T}$. The factor ϵ_F , called the quasienergy, is uniquely defined up to an integer multiple of $\frac{2\pi}{T}$. In other words, an eigenvector with quasienergy ϵ_F is associated with the eigenvectors with quasienergy $\epsilon'_F = \epsilon_F \pm N \frac{2\pi}{T}$, in which $N \in \mathbb{Z}^+$. As the result, the quasienergy is constrained within the interval $[-\frac{\pi}{T}, \frac{\pi}{T})$.

In general, the stroboscopic time-evolution operator $U(T)$ can be effectively modeled with $\exp(-iH_\epsilon T)$, where the rigorous definition of H_ϵ is given as

$$H_\epsilon = \frac{i}{T} \log_\epsilon [U(T)]. \quad (3)$$

The subscript ϵ is introduced to specify the branch cut,

$$\log_\epsilon e^{i\phi} = i\phi, \quad \text{if } \epsilon - \frac{2\pi}{T} < \phi < \epsilon. \quad (4)$$

H_ϵ is an essential ingredient in the construction of topological invariants for Floquet systems. Meanwhile, the quasienergy

ϵ_F corresponds to the eigenvalues of $H_F = H_{\epsilon=\pi}$, called the Floquet operator. In analogy to the static case, if there is nontrivial topology in the quasienergy-band of H_F , such as a nonzero Chern number or nonzero winding number, then protected edge modes at the boundary of system would be expected.

Amazingly, one of the distinguishing features of Floquet systems is the unbounded nature of their quasienergy spectrum. In particular, there are two gaps between the quasienergy band: one centered at zero quasienergy and the other centered at $\frac{\pi}{T}$. Thus, both the edge modes traversing the 0 gap or the $\frac{\pi}{T}$ gap are allowed. Different from static cases, the appearance of chiral edge modes in the Floquet systems are related to the zero Chern number of the Floquet-Bloch band, which is the anomalous chiral edge mode in the Floquet systems. To characterize those edge modes, the winding number W_ϵ is introduced [6]:

$$W_\epsilon = \int \frac{dt dk_x dk_y}{8\pi^2} \text{Tr} (U_\epsilon^{-1} \partial_t U_\epsilon [U_\epsilon^{-1} \partial_{k_x} U_\epsilon, U_\epsilon^{-1} \partial_{k_y} U_\epsilon]), \quad (5)$$

where the modified time-evolution operator is defined as

$$U_\epsilon = U(t) \exp(iH_\epsilon t), \quad (6)$$

and the ordinary time-evolution operator is $U(t) = \hat{\mathcal{T}} \exp(-i \int_0^t H(t') dt')$. The winding numbers W_0 and W_π respectively associated with the 0 gap and π gap, and the Chern number of the lower Floquet-Bloch band ($\epsilon_F < 0$) is given as

$$C_F = W_\pi - W_0. \quad (7)$$

As a result, when $W_0 = W_\pi = \pm 1$, the corresponding edge modes are anomalous. However, when $W_0 \neq W_\pi$, the anomalous chiral edge modes are absent. In this paper we find that the anomalous modes appear only if the 0 modes and π modes possess the same chirality; on the contrary, the anomalous chiral edge modes disappear if the chirality of 0 modes and π modes are opposite.

In this paper we focus on a scenario in which the system experiences periodic impulses, leading to a Hamiltonian of the form

$$H(t) = H_0 + \sum_{l \in \mathbb{Z}} \delta(t/T - l) H_1. \quad (8)$$

This Hamiltonian gives rise to the time-evolution operator [19],

$$U(T) = \exp(-iH_0 T) \exp(-iH_1 T) = \exp(-iH_F T). \quad (9)$$

Then H_F can be obtained by using the Baker-Campbell-Hausdorff (BCH) formula (Appendix A). For simplicity, we set $T = 1$ in the following discussions, that $U = e^{-iH_0} e^{-iH_1} = e^{-iH_F}$.

III. THE PERIODICALLY KICKED QI-WU-ZHANG MODEL

The topology in topological insulators is characterized by the irreducible description of its Dirac mass matrix [20]. However, the question of how topology is modified when the Dirac mass experiences periodic perturbations remains an open issue. For instance, let us consider the QWZ model [21]

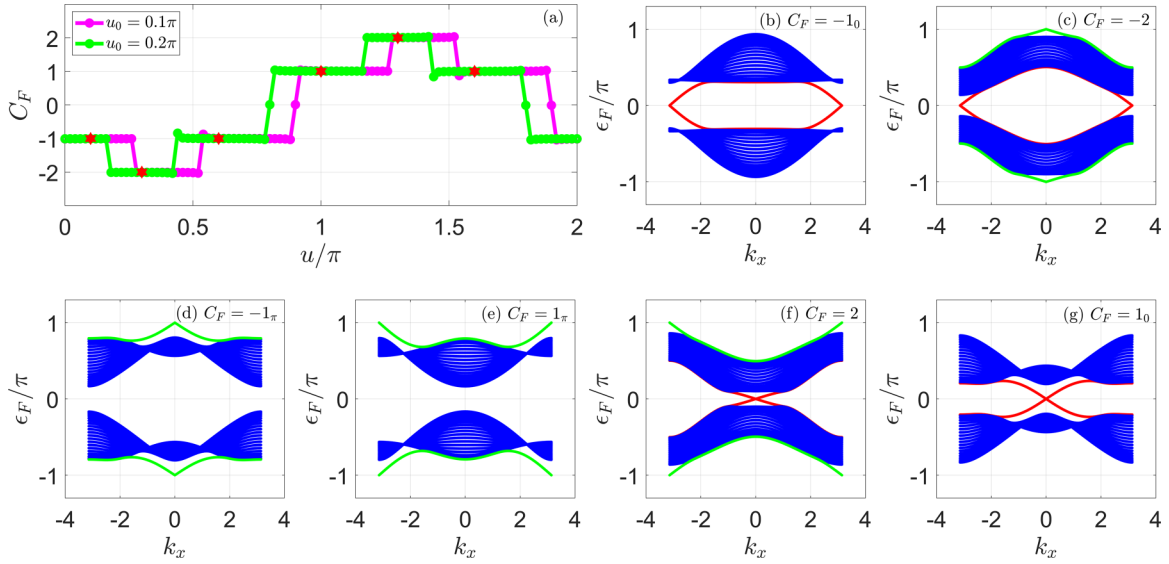


FIG. 1. (a) Chern number C_F as a function of u for $u_0 = 0.1\pi$ and $u_0 = 0.2\pi$ in the PK-QWZ model. The quasibands of the PK-QWZ model for $u = 0.1\pi$ (b), $u = 0.3\pi$ (c), $u = 0.6\pi$ (d), $u = \pi$ (e), $u = 1.3\pi$ (f), and $u = 1.6\pi$ (g) are separate, where $u_0 = 0.2\pi$, $L_y = 20$. The boundary condition along the x direction is periodic. For the topological phases with $C_F = \pm 1$, there are two chiral edge modes, either traversing the 0 gap (marked in red) or traversing the π gap (marked in green). For the topological phases with $C_F = \pm 2$, there are four chiral edge modes. They are separated into two pairs, one pair traverses the 0 gap and the other traverses the π gap.

in which the Bloch Hamiltonian is

$$H_{\text{qwz}}(\mathbf{k}) = \sin k_x \sigma_x + \sin k_y \sigma_y + (u_0 + \cos k_x + \cos k_y) \sigma_z. \quad (10)$$

The Pauli matrices $\sigma_{x,y,z}$ represent the internal degrees of freedom in each unit cell; we assume it is the spin degrees of freedom (\uparrow, \downarrow) in this paper. It is easy to find that $H_{\text{qwz}}(\mathbf{k})$ is particle-hole symmetric,

$$\sigma_x H_{\text{qwz}}^T(-\mathbf{k}) \sigma_x = -H_{\text{qwz}}(\mathbf{k}), \quad (11)$$

which belongs to class D and has \mathbb{Z} classification in the two-dimensional (2D) case. And its topology is captured by the Chern number C_{qwz} , which is equal to the integration of the Berry curvature across the whole Brillouin zone (BZ) for its lower energy band. Specifically, $C_{\text{qwz}} = +1$ for $0 < u_0 < 2$, $C_{\text{qwz}} = -1$ for $-2 < u_0 < 0$, while $C_{\text{qwz}} = 0$ for $|u_0| > 2$ [21]. The Dirac mass matrix of the QWZ model is σ_z . Then, assume that $H_0 = H_{\text{qwz}}(\mathbf{k})$ and $H_1 = u\sigma_z$, where its topology has been discovered in Refs. [22,23]. Here we study it further by considering the topology of the Floquet band and the details of topological phase transitions.

By substituting H_0 and H_1 in Eq. (9), one can find the Floquet operator $H_F(\mathbf{k})$ of the periodically kicked QWZ (PK-QWZ) model by using the BCH formula. Then, how the topological properties of the system are affected can be understood by consulting the topology of $H_F(\mathbf{k})$. Interestingly, it is easy to find that $\sigma_x H_F^T(-\mathbf{k}) \sigma_x = -H_F(\mathbf{k})$. Consequently, the symmetry of $H_F(\mathbf{k})$ is the same as $H_{\text{qwz}}(\mathbf{k})$, and it belongs to class D as well. Then the topology contained in the quasienergy band of $H_F(\mathbf{k})$ can be extracted by a Chern number, C_F , in which the Berry curvature is defined in its lower quasienergy band (i.e., for $\epsilon_F < 0$). Moreover, the topology of $H_F(\mathbf{k})$ is decoded in its algebraic structure, which can be

formally written as

$$H_F(\mathbf{k}) = \xi(\mathbf{k}) \mathbb{1}_{2 \times 2} + \mathbf{n}(\mathbf{k}) \cdot \vec{\sigma}. \quad (12)$$

From the BCH formula, it is evident that $\xi(\mathbf{k}) = 0$. Then the quasienergy spectrum of the PK-QWZ model is

$$\epsilon_{\mathbf{k}} = \sqrt{[n^x(\mathbf{k})]^2 + [n^y(\mathbf{k})]^2 + [n^z(\mathbf{k})]^2}. \quad (13)$$

The Chern number corresponds to the winding number of the mapping from the BZ to the vector space $\hat{\mathbf{n}}(\mathbf{k})$, defined as

$$\mathbf{k} \rightarrow \hat{\mathbf{n}}(\mathbf{k}) = \frac{\mathbf{n}(\mathbf{k})}{|\mathbf{n}(\mathbf{k})|}. \quad (14)$$

In geometric terms, this is equivalent to counting the number of skyrmions in the manifold of vector space $\hat{\mathbf{n}}(\mathbf{k})$, which can be expressed as

$$C_F = \frac{1}{4\pi} \int d^2\mathbf{k} \left(\frac{\partial \hat{\mathbf{n}}(\mathbf{k})}{\partial k_x} \times \frac{\partial \hat{\mathbf{n}}(\mathbf{k})}{\partial k_y} \right) \cdot \hat{\mathbf{n}}(\mathbf{k}). \quad (15)$$

And because the unit vector $\hat{\mathbf{n}}(\mathbf{k})$ resides on a unit sphere S^2 , then C_F is equal to the times that $\hat{\mathbf{n}}(\mathbf{k})$ winds around S^2 as well.

Unfortunately, the exact expression of $H_F(\mathbf{k})$ is impossible by using the BCH formula (Appendix A). Nevertheless, the value of C_F can be determined numerically, see Fig. 1(a). When $C_F = \pm 2$ ($W_\pi = -W_0 = \pm 1$), it is expected to find four chiral edge modes. These edge modes form two pairs, one pair traversing the 0 gap and another pair traversing the π gap, as depicted in Figs. 1(c) and 1(f). Surprisingly, there are two phases for $C_F = -1$, denoted as -1_0 and -1_π . The edge modes traverse the 0 gap for the phase $C_F = -1_0$

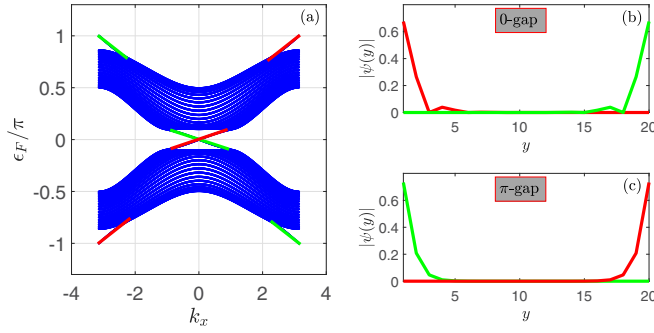


FIG. 2. Quasienergy spectrum of the PK-QWZ model for $C_F = 2$ (a), where the boundary condition along the x direction is periodic, $L_y = 20$, $u = 1.3\pi$, and $u_0 = 0.2\pi$. Also presented are the chiral edge modes traversing the 0 gap (b) and the chiral edge modes traversing the π gap (c), where $|\psi(y)|^2 = |\psi(y)_r|^2 + |\psi(y)_l|^2$. For the right-handed edge modes, those traversing the 0 gap are localized at $y = 1$ (b, red solid line), while those traversing the π gap are localized at $y = L_y$ (c, green solid line). And the left-handed chiral edge modes (dashed line) are the other way around.

($W_\pi = 0, W_0 = 1$), while the edge modes traverse the π gap for the phase $C_F = -1_\pi$ ($W_\pi = -1, W_0 = 0$), see Figs. 1(b) and 1(d). And there are two phases for $C_F = 1$ as well, denoted as 1_0 and 1_π , see Figs. 1(e) and 1(g).

With the above observations, we can understand the anomalous chiral edge modes in terms of Berry curvature as well, where C_F corresponds to the integral of Berry curvature across the BZ for the lower quasienergy band (i.e., $\epsilon_F < 0$). However, the lower quasienergy band is the upper quasienergy band of the chiral edge mode traversing the π gap, such that the Chern number is zero if the 0 modes have the same chirality as the π modes. In other words, if the chirality of the 0 modes are the same as the π modes, then the corresponding signs of winding numbers for these two edge modes are opposite. Fortunately, the anomalous chiral edge modes are absent in the PK-QWZ model. When the 0 and π modes exist simultaneously, their chiralities are different from each other. Specifically, for the case $C_F = 2$, we find two edge modes which have opposite chirality; one of them traverses the 0 gap and the other the π gap, as illustrated in Figs. 2 and 3.

For the sake of brevity, we will use Chern number C_F to characterize the topological phases of the PK-QWZ model in the following discussions.

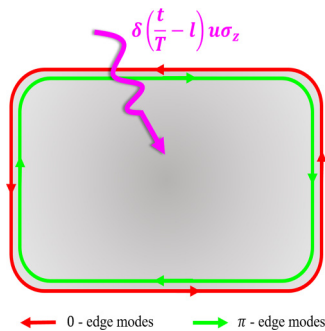


FIG. 3. Graphical representation of chiral edge modes in PK-QWZ model for $C_F = 2$.

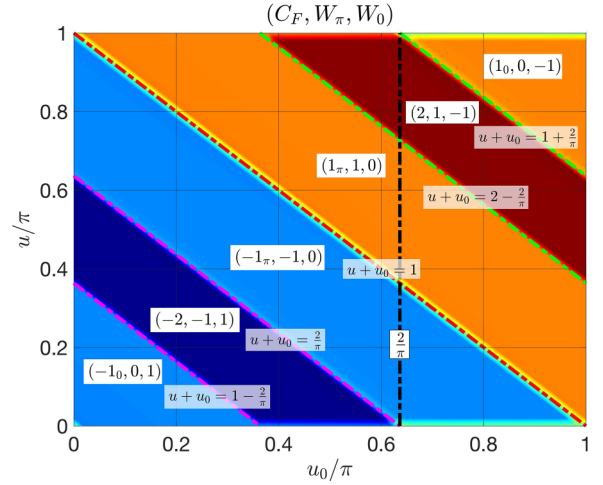


FIG. 4. Phase diagram of the PK-QWZ model: the magenta dashed lines represent the phase boundaries between the phase with $C_F = -2$ and those with $C_F = -1_s$, the red dashed lines are the phase boundaries between the phase with $C_F = -1_\pi$ and those with $C_F = 1_\pi$, green dashed lines mark the phase boundaries between the phase with $C_F = 2$ and those with $C_F = 1_s$, and black dashed line is the critical point of the static QWZ model, where $u_0 = 2$, and where $s = 0$ or π .

IV. PHASE DIAGRAM OF PERIODICALLY KICKED QI-WU-ZHANG MODEL

The phase diagram of the PK-QWZ model is depicted in Fig. 4, illustrating the variation of the Chern number C_F with respect to u_0 and u . As mentioned before, the Chern number is equal to the numbers of skyrmions (N_{sky}) in the vector space of $\hat{\mathbf{n}}$ [21], in which the base manifold is the BZ. In this context, the phases $C_F = \pm 1$ correspond to the situation that the vector $\hat{\mathbf{n}}$ winds around the unit sphere S^2 once, while the phases $C_F = \pm 2$ represent that the vector $\hat{\mathbf{n}}$ winds around the unit sphere S^2 twice. In other words, the phase diagram also reflects the variation of N_{sky} over the parameters u_0 and u . And the phase boundaries can be uncovered by investigating the number of skyrmions in the vector space $\hat{\mathbf{n}}$.

Despite the absence of the exact expression for $H_F(\mathbf{k})$, the low-energy effective theory is sufficient to capture the topology of $H_F(\mathbf{k})$. In the low-energy limit, $H_F(\mathbf{k})$ reduces to a Dirac Hamiltonian with the momentum matrices σ_x and σ_y , while the mass matrix is σ_z (see Appendix A). Thus, N_{sky} is entirely determined by the variation of $n^z(\mathbf{k})$ over the BZ; to be precise, N_{sky} is equal to the number of times that the sign of $n^z(\mathbf{k})$ changes in the BZ. There are two specific points in the BZ that need consideration. The first one, denoted as a Γ -type point, corresponds to points $(k_x, k_y) = (0, 0)$ and (π, π) ; the second one, denoted as a Λ -type point, is located at $(k_x, k_y) = (0, \pi)$ and $(\pi, 0)$. For the Γ type, we have

$$n_{\Gamma, \pm}^z = u + u_0 \pm 2, \quad (16)$$

where “+” is for $(0,0)$ and “-” is for (π, π) . For Λ type, we have

$$n_{\Lambda}^z = u + u_0. \quad (17)$$

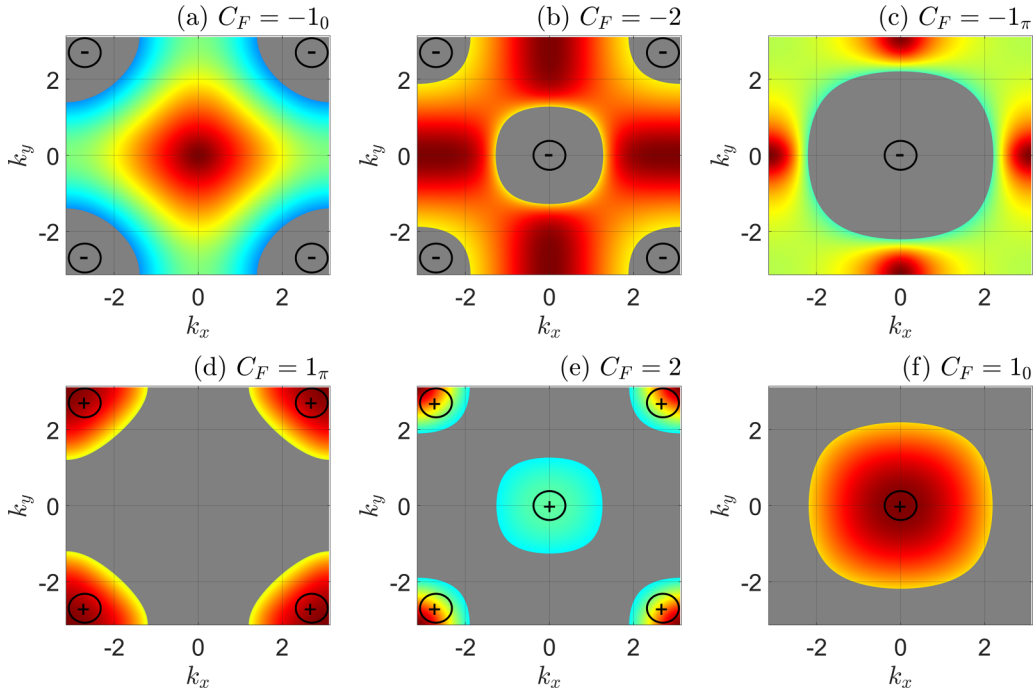


FIG. 5. Contour plot of $n_z(k_x, k_y)$ for different values of u , where $u_0 = 0.2\pi$. The presented cases are for $u = 0.1\pi$ (a), $u = 0.3\pi$ (b), $u = 0.6\pi$ (c), $u = \pi$ (d), $u = 1.3\pi$ (e), and $u = 1.6\pi$ (f) separately. In these plots the gray areas represent regions where $n^z < 0$. The phases $C_F = \pm 1$ are for the case that the sign of n^z changes only once in the BZ (a), (c), (d), (f), while the phases with $C_F = \pm 2$ are for the case that the sign of n^z changes twice in the BZ (b), (e).

As a result, N_{sky} is obtained by identifying the variation of $n_{\Gamma_{\pm}}^z$ and n_{Λ}^z as u_0 and u are varied. When $-2 < u + u_0 < \pi - 2$, it is evident that $n_{\Lambda}^z > 0$, $n_{\Gamma_{+}}^z > 0$, and $n_{\Gamma_{-}}^z < 0$. In this case, the sign of n_z changes only once in the BZ, leading to $N_{\text{sky}} = 1$, corresponding to the topological phase with $C_F = -1_0$, as depicted in Fig. 5(a). When $\pi - 2 < u + u_0 < 2$, we find that $n_{\Lambda}^z > 0$ and $n_{\Gamma_{\pm}}^z < 0$. In this situation, the sign of n_z changes twice in the BZ, resulting in $N_{\text{sky}} = 2$, which corresponds to the topological phase with $C_F = -2$, see Fig. 5(b). So the phase boundary between the phase $C_F = -1_0$ and the phase $C_F = -2$ is $u + u_0 + 2 = \pi$, as depicted in Fig. 4, in which the π gap is closed at the point $(k_x, k_y) = (0, 0)$. As $u + u_0$ increases, that $2 < u + u_0 < \pi$, we find that $n_{\Lambda}^z > 0$, $n_{\Gamma_{+}}^z < 0$, and $n_{\Gamma_{-}}^z > 0$. In this case the sign of n_z changes only once in the BZ, leading to $N_{\text{sky}} = 1$, which corresponds to the topological phase with $C_F = -1_{\pi}$, see Fig. 5(c). Consequently, the phase boundary between the phase $C_F = -2$ and the phase $C_F = -1_{\pi}$ is $u + u_0 = 2$, as presented in Fig. 4, in which the 0 gap is closed at the point $(k_x, k_y) = (\pi, \pi)$.

As $u + u_0$ increases further, that $\pi < u + u_0 < 2\pi - 2$, we find that $n_{\Lambda}^z < 0$, $n_{\Gamma_{+}}^z < 0$ and $n_{\Gamma_{-}}^z > 0$. In this case the sign of n_z changes only once in the BZ, leading to $N_{\text{sky}} = 1$, which corresponds to the topological phase with $C_F = 1_{\pi}$, see Fig. 5(d). Consequently, the phase boundary between the phase $C_F = -1_{\pi}$ and the phase $C_F = 1_{\pi}$ is $u + u_0 = \pi$, as presented in Fig. 4, in which the π gap is closed at points $(k_x, k_y) = (0, \pi)$ and $(\pi, 0)$. With the same approach, all configurations of $n_{\Gamma_{\pm}}^z$ and n_{Λ}^z for different topological phases are uncovered, which is summarized in Table I. And the phase boundaries are determined by the critical point where $n_{\Gamma_{\pm}}^z$ or n_{Λ}^z changes sign, see Table II.

V. VON NEUMANN ENTROPY OF FLOQUET STEADY STATE IN PK-QWZ MODEL

A quantum system never completely decouples from its environment so that the thermalization or the dissipation finally leads the system relax to a stationary state. However, not much is known about the stationary states of periodically driven systems. Related research has been a very hot topic recently, for example, the quantum time crystal [24,25]. Furthermore, the study of the thermodynamic properties of the Floquet system is of great importance; relevant research involves the unique Floquet-Gibbs state [26–29] and the exceptional selection rules [30].

In this section we want to investigate the orders of the topological phase transition in the PK-QWZ model. The difficulties in finding the ground state of the Floquet system are resolved by considering the stationary state of the corresponding open quantum system, which corresponds to a situation

TABLE I. The sign of mass n^z at Λ points and Γ points for different topological states, where “+” is for $n^z > 0$, and “-” is for $n^z < 0$.

C_F	$n_{\Gamma_{+}}^z$	n_{Λ}^z	$n_{\Gamma_{-}}^z$	N_{sky}
-1_0	+	+	-	1
-2	-	+	-	2
-1_{π}	-	+	+	1
1_{π}	-	-	+	1
2	+	-	+	2
1_0	+	-	-	1

TABLE II. The phase boundaries, the types of quasienergy gap (q. g.) that are closed, the points where the quasienergy gap is closed in the BZ, and the order of phase transition (OPT) with respect to u and u_0 , respectively, where “\” means that the phase of FSS is not well defined.

Phase 1 & Phase 2	Phase boundary	q. g.	Transition point (k_x, k_y)	OPT vs u	OPT vs u_0
$C_F = -1_0$ & $C_F = -2$	$u + u_0 + 2 = \pi$	π	Γ_+	2	2
$C_F = -2$ & $C_F = -1_\pi$	$u + u_0 = 2$	0	Γ_-	3	3
$C_F = -1_\pi$ & $C_F = 1_\pi$	$u + u_0 = \pi$	π	Λ	3	1
$C_F = 1_\pi$ & $C_F = 2$	$u + u_0 + 2 = 2\pi$	0	Γ_+	2	\
$C_F = 2$ & $C_F = 1_0$	$u + u_0 = 2 + \pi$	π	Γ_-	3	\
$C_F = 1_0$ & $C_F = -1_0$	$u + u_0 = 2\pi$	0	Λ	3	\

where the periodically driven system is weakly coupled to a Markovian environment and the system will finally relax into a stationary state. Then the orders of topological phase transition can be determined by studying the properties of FSS.

If the Hamiltonian of an open quantum system is time dependent, then the time evolution of the system can be described with a time-dependent Lindblad master equation [31],

$$\frac{d}{dt}\rho = -i[H(t), \rho] + \sum_{\mu} (2L_{\mu}^{\dagger}\rho L_{\mu} - \{L_{\mu}^{\dagger}L_{\mu}, \rho\}), \quad (18)$$

in which L_{μ} corresponds to the gain or loss of particles due to the coupling to the environment. For a lattice model, the general form of the Lindblad operator is

$$L_j^g = \sum_s D_{j,s}^g c_{j,s}^{\dagger}, \quad L_j^l = \sum_s D_{j,s}^l c_{\mu,s}, \quad (19)$$

where j is the site index and s corresponds to the internal degrees of freedom for each lattice site.

Due to the Gaussian quadratic property of free fermionic systems, its dynamics is described with the single-particle correlation matrix [32,33],

$$i\frac{d}{dt}C(t) = X(t)C(t) - C(t)X(t)^{\dagger} + 2iM_g, \quad (20)$$

where $C_{mn} = \langle c_m^{\dagger} c_n \rangle$, in which $X(t)$ is the time-dependent damping matrix

$$X(t) = -H^T(t) - i(M_g + M_l^T), \quad (21)$$

where the non-Hermitian terms M_g and M_l are induced by the coupling with the environment, where

$$(M_g)_{ij} = \sum_{\mu} D_{\mu i}^{g*} D_{\mu j}^g, \quad (M_l)_{ij} = \sum_{\mu} D_{\mu i}^{l*} D_{\mu j}^l. \quad (22)$$

In the case of a periodically kicked free fermionic system, we found that its single-particle correlation matrix of FSS satisfies a standard Sylvester equation (Appendix B),

$$e^{iX_1 T} P_- = e^{iX_1 T} e^{iX_0 T} C^{F,s} - C^{F,s} e^{iX_1^{\dagger} T} e^{iX_0^{\dagger} T}, \quad (23)$$

where $C^{F,s}$ is the single-particle correlation matrix of FSS. Here, $X_0 = -H_0^T - i(M_g + M_l^T)$, $X_1 = -H_1^T$, $P_- = e^{iX_0 T} C^s - C^s e^{iX_0^{\dagger} T}$ is related to the static stationary states C^s (see Appendix B), and the superscript H_0^T represents the transposition of H_0 . This equation is usually solved with the iteration method [34,35]. Here, we numerically solve it by using the toolbox in MATLAB, the **lyap**, where the corresponding algorithm is the iteration method. However, there is no reason

to expect that $C^{F,s}$ reduces to C^s as $u = 0$. This is because that there is a time-evolution factor $e^{-iX_0 T}$ in the Sylvester equation (23) which distinguishes itself from the static systems.

We introduce the Lindblad operator as

$$L_j^g = \sqrt{\gamma} c_{j,\uparrow}^{\dagger}, \quad L_j^l = \sqrt{\gamma} c_{j,\downarrow}, \quad (24)$$

where j is the site index. Due to the coupling with the environment, the occupation of particles with up-spin is boosted, while the particles with down-spin are dissipated away, as presented in Fig. 6. Thus the non-Hermitian terms in X_0 are

$$M_g = \mathbb{1}_{L_x \times L_y} \otimes \begin{pmatrix} 1 & 0 \\ 0 & 0 \end{pmatrix}, \quad M_l = \mathbb{1}_{L_x \times L_y} \otimes \begin{pmatrix} 0 & 0 \\ 0 & 1 \end{pmatrix}. \quad (25)$$

As a result, $X_0 = -H_{\text{qWZ}}^T - i\gamma\mathbb{1}$, which leads to

$$e^{iX_1 T} e^{iX_0 T} = e^{iH_F^T T} e^{\gamma T}, \quad (26)$$

$$e^{iX_1^{\dagger} T} e^{iX_0^{\dagger} T} = e^{iH_F^{\dagger} T} e^{-\gamma T}. \quad (27)$$

It is obvious that the eigenvalues of $e^{iH_F^T T} e^{\gamma T}$ are distinct from those of $e^{iH_F^{\dagger} T} e^{-\gamma T}$, so there have only one solution for the Sylvester equation in Eq. (23) [36].

The single-particle correlation matrix $C^{F,s}$ is a key quantity that has direct connections to various aspects of the system. It is related to the occupation numbers of particles, the von Neumann entropy, and the particle currents in the system. Among these quantities, the von Neumann entropy is particularly significant, as it serves as an important measure for understanding the phase transition in the FSS. The von

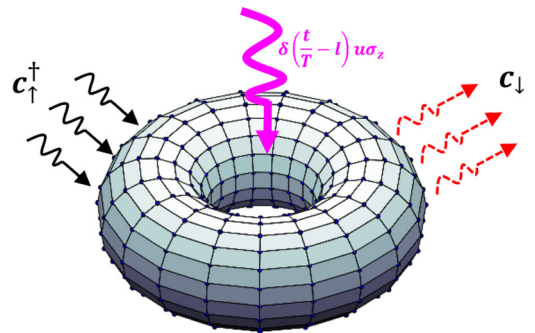


FIG. 6. Pictorial illustration of the PK-QWZ model weakly coupled to the Markovian environment, where the occupation of particles with up-spin is boosted while the particles with down-spin are dissipated away. The geometry of system is a torus where the boundary conditions are periodic both for the x and y directions.

Neumann entropy is defined as $S = -\text{Tr}(\rho \ln \rho)$, which is used to quantify the amount of quantum information contained in a many-body quantum state. $S = 0$ for a pure state, $S = 1$ for the maximally mixed state, while $0 < S < 1$ for a general mixed state. This information-theoretic entropy is a good candidate for thermodynamic entropy [37], where the singularities of S are also a good signature of phase transition. In a free fermionic system, the von Neumann entropy of its subsystem is related to the eigenvalues of its corresponding single-particle correlation matrix $C_{ij} = \langle c_i^\dagger c_j \rangle$, which is given by [38]

$$S = - \sum_j [\xi_j \ln \xi_j + (1 - \xi_j) \ln(1 - \xi_j)], \quad (28)$$

where ξ_j are the eigenvalues of C . Then, by regarding ρ as a subsystem of system ρ_{s+E} , Eq. (28) is valid to evaluate the von Neumann entropy of ρ as well.

Thus when $C^{F,s}$ is obtained, the von Neumann entropy of the FSS can be obtained by using Eq. (28). One thing to note is that the bulk property is vital to reflect the main feature of the phase transition. So the geometry of system is assumed as a torus where both boundary conditions along the x and y directions are periodic, as depicted in Fig. 6. Here we are focus on the average value of von Neumann entropy,

$$\bar{S} = \frac{1}{2L_x L_y} \frac{S}{\ln 2}, \quad (29)$$

where S is the von Neumann entropy of FSS, and L_x and L_y are the length of torus along the x and y directions, respectively. The factor $1/\ln 2$ is introduced to normalize the von Neumann entropy.

In Fig. 7 we present the dependence of average von Neumann entropy \bar{S} of the FSS on the parameter u , where u_0 is fixed. Notably, we observe a periodic behavior of \bar{S} as a function of u , with a period of π . This periodic pattern is a direct consequence of the periodic nature of the Sylvester equation in Eq. (23), which possesses an intrinsic π periodicity with respect to u . Furthermore, within the topological phase characterized by $C_F = \pm 2$, \bar{S} features a plateau. And \bar{S} reaches the maximum value precisely at the critical points marking the transition between phases with $C_F = \pm 1_{0,\pi}$ and those with $C_F = \mp 1_{0,\pi}$, as presented in Fig. 7(a). Remarkably, the discontinuities that emerge in the derivatives of \bar{S} with respect to u precisely coincide with critical points separating different topological phases. We find that $\partial_u^2 \bar{S}$ is discontinuous, both for the critical point that separates the phases with $C_F = -1_0$ and $C_F = -2$, as well as the critical point between the phases with $C_F = 1_\pi$ and $C_F = 2$, which means that they are the second-order phase transitions with respect to u . Additionally, $\partial_u^3 \bar{S}$ represents the discontinuities at the critical point that separates the phases with $C_F = -1_\pi$ and $C_F = -2$, the critical point between the phases with $C_F = 1_0$ and $C_F = 2$, as well as the critical point between the phases with $C_F = \pm 1_{0,\pi}$ and $C_F = \mp 1_{0,\pi}$, which implies that they are third-order phase transitions with respect to u . A comprehensive summary of the phase transition can be found in Table II.

The dependence of average von Neumann entropy \bar{S} of FSS vs u_0 is studied as well, where u is fixed. The results

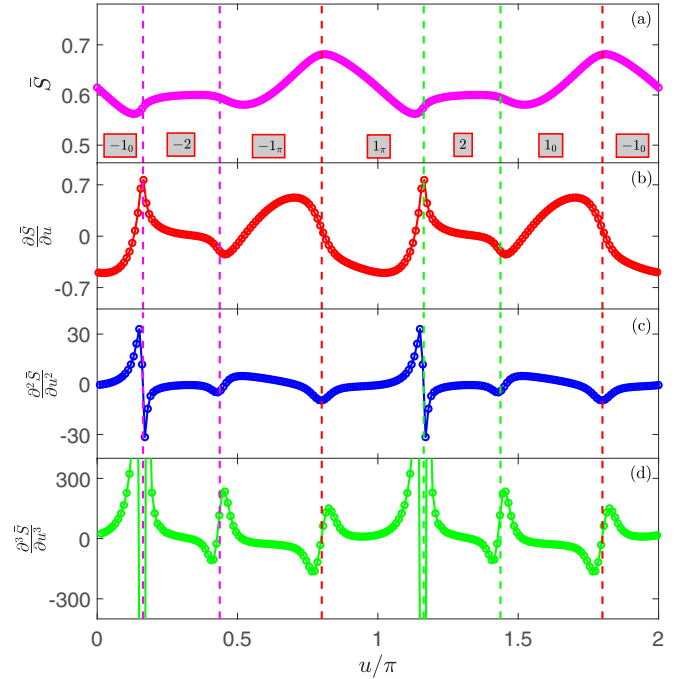


FIG. 7. Average von Neumann entropy \bar{S} vs u_0 (a) of FSS in the toruslike PK-QWZ model, and the first-order (b), second-order (c), and third-order (d) derivatives of \bar{S} with respect to u , where $u_0 = 0.2\pi$, $\gamma = 0.002$, and $L_x = L_y = 30$. It worth noting that \bar{S} is periodic in u with a period of π .

reveal a decreasing tendency of \bar{S} as u_0 is increasing, as depicted in Fig. 8(a). Notably, it is observed that the phases of FSS are well defined only if $u_0 \leq 2\pi - 2 - u$. Otherwise, the derivation of \bar{S} with respect to u_0 exhibits chaotic behavior, and then phases of FSS are ill defined. We find that $\partial_{u_0} \bar{S}$ exhibits a discontinuity at the critical point between the phases with $C_F = -1_\pi$ and $C_F = 1_\pi$, indicating a first-order phase transition with respect to u_0 , see Fig. 8(b). Additionally, $\partial_{u_0}^2 \bar{S}$ exhibits a discontinuity at the critical point between the phases with $C_F = -1_0$ and $C_F = -2$, marking a second-order phase transition with respect to u_0 , see Fig. 8(c). Finally, $\partial_{u_0}^3 \bar{S}$ exhibits a discontinuity at the critical point between the phases with $C_F = -2$ and $C_F = -1_\pi$, indicating a third-order phase transition with respect to u_0 , see Fig. 8(d). These findings are summarized in Table II.

The orders of phase transition are fixed either at the Γ point $[(k_x, k_y) = (0, 0) \text{ or } (\pi, \pi)]$ or at the Δ point $[(k_x, k_y) = (0, \pi) \text{ or } (\pi, 0)]$ in the static TIs [39], while the orders of phase transition versus u at the Γ point are different from those at the Δ point. This is attributed to the structure of the time-evolution operator in Eq. (9), that the time-dependent term H_1 is the Dirac mass term of the system, and the low-energy expansion of momentum only involves the static part H_0 . In the low-energy limit, the algebraic structures of $e^{-iH_0 T}$ at the Γ_+ point are different from those at the Γ_- point, for example, $e^{-iH_0 T} \rightarrow e^{-i(u_0+2)\sigma_z}$ as $(k_x, k_y) \rightarrow (0, 0)$ and $e^{-iH_0 T} \rightarrow e^{-i[\pi\sigma_x + \pi\sigma_y + (u_0-2)\sigma_z]}$ as $(k_x, k_y) \rightarrow (\pi, \pi)$. As a result, the algebraic structure of the Floquet operator $H_F(\mathbf{k})$ is different for different quasienergy gap closing points, and thus the orders of phase transition are different, see Table II.

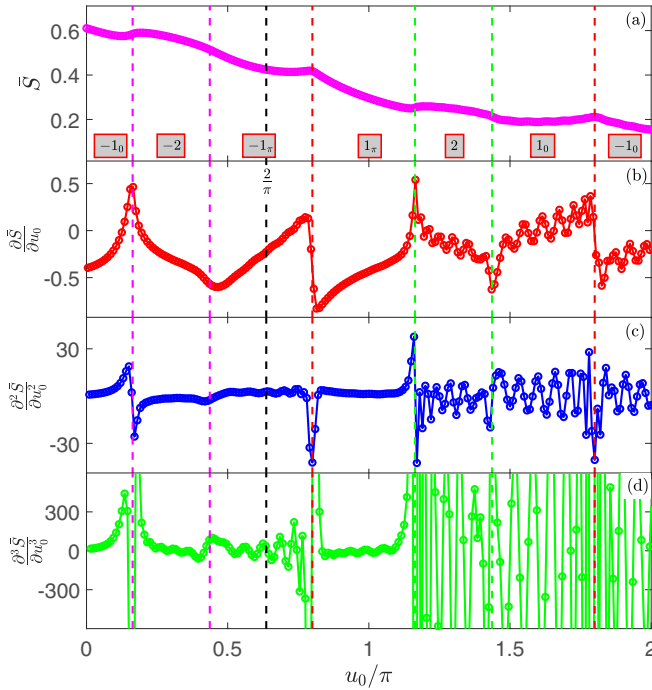


FIG. 8. Average von Neumann entropy \bar{S} vs u_0 (a) of FSS in the toruslike PK-QWZ model, and the first-order (b), second-order (c), and third-order (d) derivatives of \bar{S} with respect to u_0 , where $u = 0.2\pi$, $\gamma = 0.002$, and $L_x = L_y = 30$. Moreover, \bar{S} decreases as u_0 increases, and well-defined phases only exist when $u_0 < 2\pi - 2 - u$ because the derivative of \bar{S} with respect to u_0 becomes chaotic beyond this limit.

VI. CONCLUSION AND DISCUSSION

Key features of the periodically kicked Dirac mass term in the Chern insulators are revealed in this paper. We find that the chirality of the edge modes traversing the 0 gap are opposite to those traversing the π gap, such that the anomalous chiral edge modes are absent in this system. As a result, there are six distinct topological phases in the PK-QWZ model, denoted as $C_F = \{-1_0, -2, -1_\pi, 1_\pi, 2, 1_0\}$. Despite this, the mechanism of its unique topology is uncovered with the effective low-energy Dirac Hamiltonian, and the phase boundaries between different topological phases are explicitly found. Additionally, with the help of the time-dependent Lindblad master equation, we derived a Sylvester equation (23) of FSS for the periodically kicked free fermionic system. Then, by studying the von Neumann entropy of FSS in the PK-QWZ model, we unveil the orders of phase transitions between different topological phases, which are summarized in Table II.

As a step forward, the features of periodically kicked Dirac mass in other topological matters is waiting to be discovered, such as the \mathbb{Z}_2 TIs and topological superconductors, which is our future research direction.

ACKNOWLEDGMENTS

This work is supported by the National Natural Science Foundation of China (Grant No. 11974053 and No. 12174030) and the National Key R&D Program of China

(Grant No. 2023YFA1406704). We thank Ji-Yao Fan and Wu-Ming Liu for the helpful discussion.

APPENDIX A: APPROXIMATE EXPRESSION OF FLOQUET OPERATOR

The Euler equation directly leads to

$$\exp(i\phi\hat{\mathbf{n}} \cdot \vec{\sigma}) = \cos \phi + i\hat{\mathbf{n}} \cdot \vec{\sigma} \sin \phi. \quad (\text{A1})$$

We then express the Hamiltonian and the Floquet operator as

$$H_0 = E_{\mathbf{k}}(r^x\sigma_x + r^y\sigma_y + r^z\sigma_z), \quad (\text{A2})$$

$$H_F = \epsilon_{\mathbf{k}}(\hat{n}^x\sigma_x + \hat{n}^y\sigma_y + \hat{n}^z\sigma_z), \quad (\text{A3})$$

where $r^x = \frac{\sin k_x}{E_{\mathbf{k}}}$, $r^y = \frac{\sin k_y}{E_{\mathbf{k}}}$, $r^z = \frac{u_0 + \cos k_x + \cos k_y}{E_{\mathbf{k}}}$, and $(\hat{n}^x)^2 + (\hat{n}^y)^2 + (\hat{n}^z)^2 = 1$. The energy of the QWZ model is $E_{\mathbf{k}} = \sqrt{\sin^2 k_x + \sin^2 k_y + (u_0 + \cos k_x + \cos k_y)^2}$, and $\epsilon_{\mathbf{k}}$ is the quasienergy of the system, $\epsilon_{\mathbf{k}} \in [-\pi, \pi)$. Then the time-evolution operator in the PK-QWZ model can be rewritten as

$$\begin{aligned} U &= \exp[-iH_0(\mathbf{k})] \exp(-iH_1) \\ &= [\cos(E_{\mathbf{k}}) \cos u + r^z \sin(E_{\mathbf{k}}) \sin u] \\ &\quad - i\sigma_z [\cos(E_{\mathbf{k}}) \sin u + r^z \sin(E_{\mathbf{k}}) \cos u] \\ &\quad - i\sigma_x \sin(E_{\mathbf{k}}) [r^x \cos u + r^y \sin u] \\ &\quad - i\sigma_y \sin(E_{\mathbf{k}}) [r^y \cos u - r^x \sin u]. \end{aligned} \quad (\text{A4})$$

For simplicity, we denote $U(T=1)$ as U . Furthermore, an equivalent expression is $U = \exp(-iH_F)$, so $U = \cos \epsilon_{\mathbf{k}} - i(\hat{n}^x\sigma_x + \hat{n}^y\sigma_y + \hat{n}^z\sigma_z) \sin \epsilon_{\mathbf{k}}$. Thus we have the following equations:

$$\cos \epsilon_{\mathbf{k}} = \cos(E_{\mathbf{k}}) \cos u + r^z \sin(E_{\mathbf{k}}) \sin u, \quad (\text{A5})$$

$$\hat{n}^x \sin \epsilon_{\mathbf{k}} = \sin(E_{\mathbf{k}}) [r^x \cos u + r^y \sin u], \quad (\text{A6})$$

$$\hat{n}^y \sin \epsilon_{\mathbf{k}} = \sin(E_{\mathbf{k}}) [r^y \cos u - r^x \sin u], \quad (\text{A7})$$

$$\hat{n}^z \sin \epsilon_{\mathbf{k}} = \cos(E_{\mathbf{k}}) \sin u + r^z \sin(E_{\mathbf{k}}) \cos u. \quad (\text{A8})$$

In the low-energy limit that $E_{\mathbf{k}} \rightarrow 0_+$ as $(k_x, k_y) \rightarrow (0_+, 0_+)$, we have

$$\cos \epsilon_{\mathbf{k}} \simeq \cos u + (u_0 + 2) \sin u, \quad (\text{A9})$$

$$\hat{n}^x \sin \epsilon_{\mathbf{k}} \simeq k_x \cos u + k_y \sin u, \quad (\text{A10})$$

$$\hat{n}^y \sin \epsilon_{\mathbf{k}} \simeq k_y \cos u - k_x \sin u, \quad (\text{A11})$$

$$\hat{n}^z \sin \epsilon_{\mathbf{k}} \simeq \sin u + (u_0 + 2) \cos u. \quad (\text{A12})$$

Meanwhile, as the energy gap is closed, the 0 gap might be closed ($\epsilon_{\mathbf{k}} \rightarrow 0_+$) as $u \rightarrow 0_+$, so that we have $n^x \simeq k_x + uk_y$, $n^y \simeq k_y - uk_x$, $n^z \simeq u + u_0 + 2$. As a result, when the driving force is the Dirac mass term of Chern insulators, the effective low-energy theory of the Floquet operator is identical to its static counterpart, where the momentum matrices are σ_x and σ_y , and the mass matrix is σ_z .

However, the approximate formula of Floquet operator would provide more insights about the effective

low-energy physics. Here the Baker-Campbell-Hausdorff formula is used:

$$e^A e^B = \exp \left[A + B + \frac{1}{2}[A, B] + \frac{1}{12}[A, [A, B]] + \frac{1}{12}[B, [B, A]] + \frac{1}{24}[B, [A, [A, B]]] \dots \right]. \quad (\text{A13})$$

We then consider the following commutators:

$$i[-iH_{\text{qwz}}(\mathbf{k}), -iu\sigma_z] = -2u \sin k_x \sigma_y + 2u \sin k_y \sigma_x, \quad (\text{A14})$$

$$i[-iu\sigma_z, -[u\sigma_z, H_{\text{qwz}}(\mathbf{k})]] = 4u^2 \sin k_x \sigma_x + 4u^2 \sin k_y \sigma_y, \quad (\text{A15})$$

$$i[-iH_{\text{qwz}}(\mathbf{k}), -[H_{\text{qwz}}(\mathbf{k}), u\sigma_z]] = -4u(\sin^2 k_x + \sin^2 k_y)\sigma_z + 4u \sin k_x (u_0 + \cos k_x + \cos k_y)\sigma_x + 4u \sin k_y (u_0 + \cos k_x + \cos k_y)\sigma_y, \quad (\text{A16})$$

$$i[-iu\sigma_z, [-iH_{\text{qwz}}(\mathbf{k}), -[H_{\text{qwz}}(\mathbf{k}), u\sigma_z]]] = 8u^2 \sin k_x (u_0 + \cos k_x + \cos k_y)\sigma_y - 8u^2 \sin k_y (u_0 + \cos k_x + \cos k_y)\sigma_x. \quad (\text{A17})$$

Ignoring the higher-order terms, we have

$$n^x \simeq u \sin k_y \left[1 - \frac{u}{3} (u_0 + \cos k_x + \cos k_y) \right] + \frac{u \sin k_x}{3} \left(\frac{3}{u} + u + u_0 + \cos k_x + \cos k_y \right), \quad (\text{A18})$$

$$n^y \simeq -u \sin k_x \left[1 - \frac{u}{3} (u_0 + \cos k_x + \cos k_y) \right] + \frac{u \sin k_y}{3} \left(\frac{3}{u} + u + u_0 + \cos k_x + \cos k_y \right), \quad (\text{A19})$$

$$n^z \simeq u + u_0 + \cos k_x + \cos k_y - \frac{u}{3} (\sin^2 k_x + \sin^2 k_y). \quad (\text{A20})$$

As expected, the Floquet operator H_F reduces to a Dirac Hamiltonian in the low-energy limit, where the momentum matrices are σ_x and σ_y , and the mass matrix is σ_z .

So there are two kinds of points in the BZ where the quasienergy gap might close: the Γ type and the Λ type. If the quasienergy gap is closing at $(k_x, k_y) = (\pi, \pi)$ and $(k_x, k_y) = (0, 0)$, the quasienergy gap is

$$n_{\Gamma, \pm}^z = u + u_0 \pm 2, \quad (\text{A21})$$

where “+” is for $(0, 0)$, while “-” is for (π, π) . And if the quasienergy gap is closing at $(k_x, k_y) = (\pi, 0)$ and $(0, \pi)$, the quasienergy gap is

$$n_{\Lambda}^z = u + u_0. \quad (\text{A22})$$

By identifying the configuration of n^z , the topological property of H_F is settled, as demonstrated in the main text.

APPENDIX B: SYLVESTER EQUATION OF A PERIODICALLY KICKED, FREE FERMIONIC SYSTEM

The Sylvester equation for FSS is based on Eq. (20). However, because the Hamiltonian is time dependent, there is no reason to require that $\partial_t C^{F,s} = 0$, where $C^{F,s}$ is the stationary state of the Floquet open quantum system. Fortunately, it is natural to require that $C^{F,s}$ is periodic in time, i.e., $C^{F,s}(t+T) = C^{F,s}(t)$. We then introduce the matrix [40]

$$\Xi = \begin{pmatrix} X & -2iM_g \\ 0 & X^\dagger \end{pmatrix}, \quad D = \begin{pmatrix} \mathbb{1} & C \\ 0 & 0 \end{pmatrix}, \quad (\text{B1})$$

and Eq. (20) can be rewritten as

$$i \frac{d}{dt} D = [\Xi, D]. \quad (\text{B2})$$

There is a formal solution,

$$D(t) = \mathcal{T} \exp \left(-i \int_0^t d\tau \Xi(\tau) \right) D_0 \mathcal{T} \exp \left(i \int_0^t d\tau \Xi(\tau) \right), \\ = \mathcal{U}^F(t) D^s \mathcal{U}^F(-t), \quad (\text{B3})$$

where \mathcal{T} is the time-ordering operator, and $\mathcal{U}^F(t)$ is the corresponding time-evolution operator. We are interested in the time-evolution operator in a full period T ,

$$\mathcal{U}^F(T) = e^{-i\Xi_0 T} e^{-i\Xi_1 T}, \quad (\text{B4})$$

where

$$\Xi_0 = \begin{pmatrix} X_0 & -2iM_g \\ 0 & X_0^\dagger \end{pmatrix}, \quad \Xi_1 = \begin{pmatrix} X_1 & 0 \\ 0 & X_1^\dagger \end{pmatrix}, \quad (\text{B5})$$

and $X_0 = -H_0^T - i(M_g + M_l^T)$, $X_1 = -H_1^T$. Furthermore, Ξ_0 can be rewritten as

$$\Xi_0 = \begin{pmatrix} \mathbb{1} & -C^s \\ 0 & \mathbb{1} \end{pmatrix} \begin{pmatrix} X_0 & 0 \\ 0 & X_0^\dagger \end{pmatrix} \begin{pmatrix} \mathbb{1} & C^s \\ 0 & \mathbb{1} \end{pmatrix}, \quad (\text{B6})$$

where C^s satisfies the Lyapunov equation,

$$X_0 C^s - C^s X_0^\dagger = -2iM_g, \quad (\text{B7})$$

in which C^s is the single-particle correlation matrix of static stationary states. After simple algebraic derivation, we find that

$$\mathcal{U}^F(T) = \begin{pmatrix} e^{-iX_0 T} e^{-iX_1 T} & P_+ e^{-iX_1^\dagger T} \\ 0 & e^{-iX_0^\dagger T} e^{-iX_1^\dagger T} \end{pmatrix}, \quad (\text{B8})$$

$$\mathcal{U}^F(-T) = \begin{pmatrix} e^{iX_1 T} e^{iX_0 T} & e^{iX_1 T} P_- \\ 0 & e^{iX_1^\dagger T} e^{iX_0^\dagger T} \end{pmatrix}, \quad (\text{B9})$$

$$P_+ = e^{-iX_0 T} C^s - C^s e^{-iX_0^\dagger T}, \quad (\text{B10})$$

$$P_- = e^{iX_0 T} C^s - C^s e^{iX_0^\dagger T}. \quad (\text{B11})$$

Finally, if there is a FSS, it should be periodic in time with period T , i.e.,

$$D^s = \mathcal{U}^F(T) D^s \mathcal{U}^F(-T). \quad (\text{B12})$$

Then, substituting Eqs. (B8) and (B9) into Eq. (B12), we have a Sylvester equation,

$$e^{iX_1 T} P_- = e^{iX_1 T} e^{iX_0 T} C^{F,s} - C^{F,s} e^{iX_1^\dagger T} e^{iX_0^\dagger T}, \quad (\text{B13})$$

where $C^{F,s}$ is the single-particle correlation matrix of FSS.

-
- [1] X.-L. Qi and S.-C. Zhang, Topological insulators and superconductors, *Rev. Mod. Phys.* **83**, 1057 (2011).
- [2] J. Cayssol, B. Dóra, F. Simon, and R. Moessner, Floquet topological insulators, *Physica Status Solidi RRL* **7**, 101 (2013).
- [3] P. Titum, E. Berg, M. S. Rudner, G. Refael, and N. H. Lindner, Anomalous Floquet-Anderson insulator as a nonadiabatic quantized charge pump, *Phys. Rev. X* **6**, 021013 (2016).
- [4] H. Liu, I. C. Fulga, and J. K. Asbóth, Anomalous levitation and annihilation in Floquet topological insulators, *Phys. Rev. Res.* **2**, 022048(R) (2020).
- [5] A. G. Grushin, A. Gómez-León, and T. Neupert, Floquet fractional Chern insulators, *Phys. Rev. Lett.* **112**, 156801 (2014).
- [6] M. S. Rudner, N. H. Lindner, E. Berg, and M. Levin, Anomalous edge states and the bulk-edge correspondence for periodically driven two-dimensional systems, *Phys. Rev. X* **3**, 031005 (2013).
- [7] L. Zhou and D.-J. Zhang, Non-Hermitian Floquet topological matter, A review, *Entropy* **25**, 1401 (2023).
- [8] H. Wu, B.-Q. Wang, and J.-H. An, Floquet second-order topological insulators in non-Hermitian systems, *Phys. Rev. B* **103**, L041115 (2021).
- [9] J. Pan and L. Zhou, Non-Hermitian Floquet second order topological insulators in periodically quenched lattices, *Phys. Rev. B* **102**, 094305 (2020).
- [10] L. Zhou, Non-Hermitian Floquet topological superconductors with multiple Majorana edge modes, *Phys. Rev. B* **101**, 014306 (2020).
- [11] X. Zhang and J. Gong, Non-Hermitian Floquet topological phases: Exceptional points, coalescent edge modes, and the skin effect, *Phys. Rev. B* **101**, 045415 (2020).
- [12] S. Ke, W. Wen, D. Zhao, and Y. Wang, Floquet engineering of the non-Hermitian skin effect in photonic waveguide arrays, *Phys. Rev. A* **107**, 053508 (2023).
- [13] R. Roy and F. Harper, Periodic table for Floquet topological insulators, *Phys. Rev. B* **96**, 155118 (2017).
- [14] T. Kitagawa, E. Berg, M. Rudner, and E. Demler, Topological characterization of periodically driven quantum systems, *Phys. Rev. B* **82**, 235114 (2010).
- [15] F. Nathan and M. S. Rudner, Topological singularities and the general classification of Floquet-Bloch systems, *New J. Phys.* **17**, 125014 (2015).
- [16] Y. H. Wang, H. Steinberg, P. Jarillo-Herrero, and N. Gedik, Observation of Floquet-Bloch states on the surface of a topological insulator, *Science* **342**, 453 (2013).
- [17] J. K. Asbóth, B. Tarasinski, and P. Delplace, Chiral symmetry and bulk-boundary correspondence in periodically driven one-dimensional systems, *Phys. Rev. B* **90**, 125143 (2014).
- [18] J. H. Shirley, Solution of the Schrödinger equation with a Hamiltonian periodic in time, *Phys. Rev.* **138**, B979 (1965).
- [19] L. Zhou and J. Gong, Floquet topological phases in a spin-1/2 double kicked rotor, *Phys. Rev. A* **97**, 063603 (2018).
- [20] T. Morimoto and A. Furusaki, Topological classification with additional symmetries from Clifford algebras, *Phys. Rev. B* **88**, 125129 (2013).
- [21] X.-L. Qi, Y.-S. Wu, and S.-C. Zhang, Topological quantization of the spin Hall effect in two-dimensional paramagnetic semiconductors, *Phys. Rev. B* **74**, 085308 (2006).
- [22] T. Mishra, A. Pallaprolu, T. G. Sarkar, and J. N. Bandyopadhyay, Floquet topological phase transitions in a kicked Haldane-Chern insulator, *Phys. Rev. B* **97**, 085405 (2018).
- [23] L. C. Wang, X. P. Li, and C. F. Li, Effect of periodic kicking on Chern insulators, *Phys. Rev. B* **95**, 104308 (2017).
- [24] F. Wilczek, Quantum time crystals, *Phys. Rev. Lett.* **109**, 160401 (2012).
- [25] D. V. Else, B. Bauer, and C. Nayak, Floquet time crystals, *Phys. Rev. Lett.* **117**, 090402 (2016).
- [26] T. Shirai, T. Mori, and S. Miyashita, Condition for emergence of the Floquet-Gibbs state in periodically driven open systems, *Phys. Rev. E* **91**, 030101(R) (2015).
- [27] G. Engelhardt, G. Platero, and J. Cao, Discontinuities in driven spin-boson systems due to coherent destruction of tunneling: Breakdown of the Floquet-Gibbs distribution, *Phys. Rev. Lett.* **123**, 120602 (2019).
- [28] R. Ketzmerick and W. Wustmann, Statistical mechanics of Floquet systems with regular and chaotic states, *Phys. Rev. E* **82**, 021114 (2010).
- [29] T. Shirai, J. Thingna, T. Mori, S. Denisov, P. Hnggi, and S. Miyashita, Effective Floquet-Gibbs states for dissipative quantum systems, *New J. Phys.* **18**, 053008 (2016).
- [30] G. Engelhardt and J. Cao, Dynamical symmetries and symmetry-protected selection rules in periodically driven quantum systems, *Phys. Rev. Lett.* **126**, 090601 (2021).
- [31] H.-P. Breuer, Genuine quantum trajectories for non-Markovian processes, *Phys. Rev. A* **70**, 012106 (2004).
- [32] F. Song, S. Yao, and Z. Wang, Non-Hermitian skin effect and chiral damping in open quantum systems, *Phys. Rev. Lett.* **123**, 170401 (2019).
- [33] A. Asadian, D. Manzano, M. Tiersch, and H. J. Briegel, Heat transport through lattices of quantum harmonic oscillators in arbitrary dimensions, *Phys. Rev. E* **87**, 012109 (2013).
- [34] R. H. Bartels and G. W. Stewart, Solution of the matrix equation $AX + XB = C$ (F4), *Commun. ACM* **15**, 820 (1972).
- [35] R. Zhou, X. Wang, and X.-B. Tang, A generalization of the Hermitian and skew-Hermitian splitting iteration method for solving Sylvester equations, *Appl. Math. Comput.* **271**, 609 (2015).

- [36] A. J. B. Ward, A formula for the solution of the matrix equation $AX+XB=C$, *Int. J. Math. Educ. Sci. Technol.* **20**, 583 (1989).
- [37] G. T. Landi and M. Paternostro, Irreversible entropy production: From classical to quantum, *Rev. Mod. Phys.* **93**, 035008 (2021).
- [38] P.-Y. Chang, J.-S. You, X. Wen, and S. Ryu, Entanglement spectrum and entropy in topological non-Hermitian systems and nonunitary conformal field theory, *Phys. Rev. Res.* **2**, 033069 (2020).
- [39] Z. Cai, S. Chen, S. Kou, and Y. Wang, Properties of a class of topological phase transitions, *Phys. Rev. B* **78**, 035123 (2008).
- [40] M. van Caspel, S. E. T. Arze, and I. P. Castillo, Dynamical signatures of topological order in the driven-dissipative Kitaev chain, *SciPost Phys.* **6**, 026 (2018).